Unimolecular Decomposition of the 2-Oxepinoxy Radical: A Key Seven-Membered Ring Intermediate in the Thermal Oxidation of Benzene

Michael J. Fadden and Christopher M. Hadad*

Department of Chemistry, 100 West 18th Avenue, The Ohio State University, Columbus, Ohio 43210

Received: May 8, 2000; In Final Form: June 16, 2000

The Gibbs free energy profiles for the unimolecular decomposition of the 2-oxepinoxy radical at temperatures ranging from 298 to 1250 K have been obtained using the B3LYP method. Intermediates and transition states have been obtained that link the 2-oxepinoxy radical to various products that have been experimentally observed during the thermal oxidation of benzene. The pathways explored include the rearrangement of 2-oxepinoxy radical to cyclopentadienyl radical, pyranyl radical, and various C_4, C_3, and C_2 compounds. The decomposition of 2-oxepinoxy radical for these pathways provides a mechanism that proceeds from $C_6 \rightarrow C_5 \rightarrow C_4 \rightarrow C_2$ intermediates but does not include the cyclopentadienyl radical as a required intermediate. The most viable pathway at temperatures between 1000 and 1250 K yields either the 5-oxo-2-cyclopenten-1-yl radical and CO or the vinyl radical, acetylene, and two molecules of CO as products. A mechanism to form 5-oxo-2-cyclopenten-1-yl, a possible precursor to cyclopentadienone, is compared to the pathway for cyclopentadienone formation from the decomposition of phenoxy radical to cyclopentadienyl radical and then subsequent oxidation and rearrangement.

I. Introduction

Understanding the mechanism of the oxidation of benzene at combustion temperatures, and thereby accurately modeling this important process, has been the objective of many research efforts. Initial modeling by Fujii, Asaba, and co-workers provided fairly accurate rate laws for the production of CO and C_2 compounds based on the following proposed "global mechanism":[1,2]

$$C_6H_5^{\bullet} + O_2 \rightarrow C_6H_5OO^{\bullet} \Rightarrow 2CO + C_2H_2 + C_2H_3^{\bullet}$$

The results from this work were supported by Lin and co-workers for the CO production profile.[3] However, this global mechanism is too simplistic to account for the production of the C_5, C_4, and C_3 intermediates that are experimentally observed.

In a seminal study, Glassman and co-workers developed a mechanism for benzene oxidation with the major pathways as follows:[4]

$$C_6H_6 + O_2 \rightarrow C_6H_5^{\bullet} + HO_2^{\bullet}$$

$$C_6H_5^{\bullet} + O_2 \rightarrow C_6H_5O^{\bullet} + O(^3P)$$

$$C_6H_5O^{\bullet} \rightarrow CO + C_5H_5^{\bullet}$$

$$C_5H_5^{\bullet} + O_2 \rightarrow C_5H_5O^{\bullet} + O(^3P)$$

$$C_5H_5O^{\bullet} \rightarrow CO + C_4H_5^{\bullet}$$

$$C_4H_5^{\bullet} \rightarrow C_2H_3^{\bullet} + C_2H_2$$

Modeling studies completed in an attempt to accurately predict product concentrations based on this mechanism and other experimental data have shown reasonable quantitative agreement under some conditions, but in some cases, only qualitative agreement is possible.[5,6] Most notably, the current models overpredict phenyl, phenoxy, and cyclopentadienyl radical formation.[6] On the basis of these results, some researchers have stated that other important pathways and reactions remain to be discovered.[5] This possibility has been further supported by several other thermal, oxidative decomposition experiments in which various products are observed; however, the model suggested by Glassman does not describe the formation of these products.[7−9]

In a related study of the gas-phase oxidation of C_6H_5Cl, Senkan, Gutman, and co-workers suggested two different mechanisms for phenyl radical decomposition following chlorine atom cleavage.[10] One mechanism is by β-scission of phenyl radical, and the other is a series of reactions after the oxidation of phenyl radical with the following mechanism:

$$C_6H_5^{\bullet} + O_2 \rightarrow [C_6H_5OO^{\bullet}]^{\ddagger} \rightarrow O{=}C^{\bullet}{-}CH{=}CH{-}CH{=}CH{-}CHO$$

$$O{=}C^{\bullet}{-}CH{=}CH{-}CH{=}CH{-}CHO \rightarrow CO + {}^{\bullet}CH{=}CH{-}CH{=}CH{-}CHO$$

$${}^{\bullet}CH{=}CH{-}CH{=}CH{-}CHO \rightarrow {}^{\bullet}CH{=}CH{-}CH{=}CH_2 + CO$$

$${}^{\bullet}CH{=}CH{-}CH{=}CH_2 \rightarrow C_4H_4 + H^{\bullet}$$

$${}^{\bullet}CH{=}CH{-}CH{=}CH_2 \rightarrow C_2H_2 + C_2H_3^{\bullet}$$

This ring-opening mechanism has not been further examined to determine whether it is an energetically viable pathway for the oxidation of benzene.

In a computational study based on PM3 calculations, Carpenter proposed an alternate, viable pathway for the decomposi-

* Author to whom correspondence should be addressed. E-mail: hadad.1@osu.edu. Fax: 614-292-1685.

10.1021/jp0017238 CCC: $19.00
Published on Web 07/20/2000

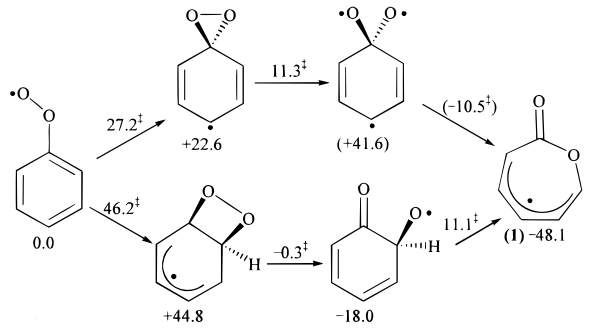

Figure 1. Unimolecular rearrangement pathways of phenylperoxy radical through a dioxiranyl or dioxetanyl radical intermediate resulting in 2-oxepinoxy radical (**1**). The relative free energies (298 K, kcal/mol) at the B3LYP/6-311+G**//B3LYP/6-31G* level are shown for each intermediate relative to phenylperoxy radical, and each free energy of activation is relative to the reactant for that specific step. See ref 13.

tion of phenylperoxy ($C_6H_5OO^{\bullet}$) radical through a dioxiranyl radical intermediate, leading to a very stable, seven-membered ring 2-oxepinoxy radical (**1**) and then further decomposition to products.[11] In subsequent studies using the B3LYP/6-31G* level, we demonstrated that the dioxiranyl radical pathway shown in Figure 1 is competitive with the phenoxy radical pathway at temperatures $\leq$1250 K, judging from Gibbs free energies for the intermediates and transition states.[12,13] We, and others, have shown that density functional theory methods can be accurately applied to benzene reactions with hydrogen atoms[14] and to aromatic radicals,[15] because spin contamination is not a significant problem as it is with some Hartree−Fock-based levels of theory.

Continuing our research into the possible pathways for the oxidation of benzene under atmospheric and combustion temperatures, we now explore the decomposition of 2-oxepinoxy radical (**1**) to a variety of products (Figure 2) that have been experimentally detected by mass spectrometric methods from benzene oxidation.[7,9] These species include cyclopentadienyl radical ($Cp^{\bullet}$, $C_5H_5^{\bullet}$, **4**), pyranyl radical (**6**), 3-oxo-1-propenyl radical (**11**), 2-cyclobuten-1-yl radical (**16**), vinyl radical ($C_2H_3^{\bullet}$, **18**), 2-cyclopenten-1-yl radical (**19**), 1,2,4-pentatrien-1-one (**22**), vinyl ketone (**25**), 4-oxo-1,3-butadienyl radical (**27**), furan (**31**), acetylene, ketene, ketenyl radical, formyl radical, CO, and CO_2, as shown in Figure 2.

II. Computational Methods

All geometry optimizations, vibrational frequency calculations, and single-point energy determinations were completed with Gaussian 94 and 98 at the Ohio Supercomputer Center or on our IBM RS/6000 workstations.[16,17]

The B3LYP/6-31G* hybrid density functional theory (DFT)[18] level was employed to determine the optimized geometries and vibrational frequencies of all stationary points.[19,20,21,22] We,[15] and others,[23] have shown that DFT methods can be used to provide accurate energies for aromatic radicals. Single-point energies were also determined at the B3LYP/6-311+G** level, as Bauschlicher and Langhoff have shown that there is a small basis set effect with oxygen-containing systems when determining C−H bond dissociation enthalpies.[24] Thus, single-point energies were also determined at the B3LYP/6-311+G** level in order to provide better relative energies. We have also determined single-point energies at the UCCSD(T)/6-31G**

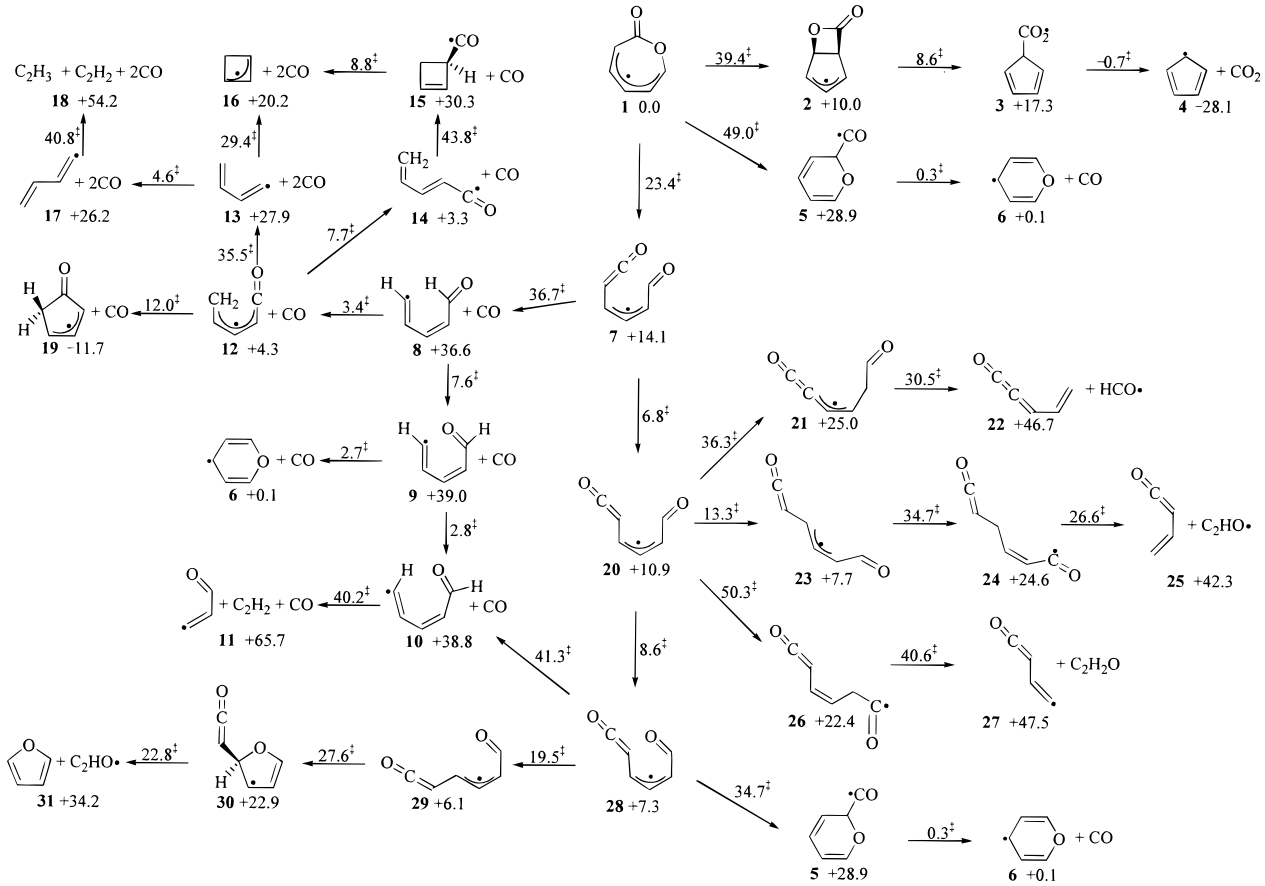

Figure 2. Unimolecular decomposition pathways of 2-oxepinoxy radical (**1**). The relative free energies (298 K, kcal/mol) at the B3LYP/6-311+G**//B3LYP/6-31G* level are shown for each intermediate relative to **1**, and each free energy of activation is relative to the reactant for that specific step.

level of theory for several key intermediates and transition states in order to compare with our B3LYP results.[25] All basis sets used six Cartesian d functions.

Vibrational frequencies were calculated for each stationary point to confirm each structure as a minimum or a saddle point, and each stationary point had the correct number of real and imaginary vibrational frequencies. The zero-point vibrational energy (ZPE) corrections were also obtained and scaled by a factor of 0.9806.[26] All transition states were confirmed to connect to the corresponding reactant and product by displacement (typically 10%) of the geometry along the reaction coordinate for the imaginary vibrational frequency in either direction, which was then followed by a careful optimization (opt = calcfc or opt = calcall) to the corresponding minimum. In some cases, intrinsic reaction coordinate (IRC) searches were used.[27]

Spin contamination for most of the stationary points is negligible. The $\langle S^2 \rangle$ values for all of the minima and transition states fell below 0.80 for the doublet species.

To determine the thermodynamic contribution to the free energy of each molecule at temperatures ranging from 298 to 2000 K, Thermo94[28] was used to calculate the partition function contributions derived from the optimized geometry and the unscaled vibrational frequencies calculated by Gaussian. The overall Gibbs free energy at each temperature was derived from the single-point energy, the scaled ZPE, the thermodynamic contribution (enthalpy and entropy), and the electronic contribution to the free energy. The only molecule that received different treatment was the O atom, for which experimentally[29] determined splitting energies were included in the electronic component of the partition function for the free energy calculation.

The energies discussed throughout (Table 1) are Gibbs free energies computed at the B3LYP/6-311+G**//B3LYP/6-31G* level (at 298 K, unless noted otherwise) and are relative to the Gibbs free energy of 2-oxepinoxy radical (**1**).

III. Reaction Mechanism and Products of 2-Oxepinoxy Radical (1) Decomposition

A. Cyclopentadienyl Radical (4) + CO_2 Formation. Through a mechanism developed by Carpenter and shown in our previous study (Figure 1), 2-oxepinoxy radical (**1**) can possibly decompose to cyclopentadienyl radical (**4**) and CO_2.[11−13] The mechanism includes the isomerization of 2-oxepinoxy radical (**1**) to the bicyclic structure 7-oxo-6-oxabicyclo[3.2.0]-hept-3-en-2-yl radical (**2**), followed by a C−O bond scission, resulting in oxomethoxy-2,4-cyclopentadien-1-yl radical (**3**), and then a facile CO_2 extrusion to yield the cyclopentadienyl radical (Cp•, **4**). The overall reaction (298 K) is −28.1 kcal/mol exoergic, with an overall free energy of activation barrier of +39.4 kcal/mol. This pathway is unique in that it provides a mechanism for prompt CO_2 emission. The formation of prompt CO_2 was noted in a study by Pfefferle and Chai where they observed "an unexpectedly high amount of CO_2 at low conversions ... suggesting that the early CO_2 has a homogeneous source."[9]

B. Pyranyl Radical (6) + CO Formation. Pyranyl radical (**6**) formation resulting from the decomposition of the 2-oxepinoxy radical (**1**) was explored along three separate pathways. The first, which has previously been examined,[12,13] results from the transformation of **1** to the pyran-1-carbonyl radical (**5**), followed by the loss of CO to produce pyranyl radical (**6**). There is very little change in the free energy (298 K) for this reaction, but the first step suffers from a free energy of activation barrier of 49.0 kcal/mol.

The second pathway investigated involves the ring opening of **1** leading to (2*Z*,4*Z*)-1,6-dioxo-2,4-hexadienyl radical (**7**), followed by CO extrusion yielding 5-oxo-1,3-pentadienyl radical (**8**), then rotation of **8** to **9**, and finally ring closure of **9** to form the pyranyl radical (**6**). As compared to the above route, this pathway suffers from a slightly higher overall free energy barrier at 298 K of 50.8 kcal/mol (relative to **1**), incurred in the loss of CO for the decomposition of **7** to **8**.

The final pathway proceeds through the ring closure of **28**, a rotamer of **7**, to form **5**, which then decomposes to pyranyl radical (**6**) and CO, as previously detailed. This pathway incurs the lowest overall free energy barrier of 42.0 kcal/mol (relative to **1**) at 298 K. The highest barrier along this path is for the ring closure of **28** to yield the intermediate **5**.

C. 3-Oxo-1-propenyl Radical (11) + Acetylene + CO Formation. Inversion at the radical center in 5-oxo-1,3-pentadienyl radical (**9**) leads to a configurational isomer, **10**, with a small free energy barrier (2.8 kcal/mol). Loss of acetylene from **10** results in the 3-oxo-1-propenyl radical (•CH═CH−CH═O, **11**). Isomer **10** can also be generated by CO loss from **28**, which is a rotamer of **7** (and **20**). In the conversion of **10** → **11**, breaking of the C−C bond to generate acetylene is significantly endoergic (ΔG = +26.9 kcal/mol) and occurs with a substantial free energy of activation barrier ($\Delta G^{\ddagger}$ = 40.2 kcal/mol). Although the free energy penalty is large at 298 K, one can expect this pathway to become more accessible as the entropic benefit is accentuated by increasing temperature. It is also highly likely that a low-energy pathway also exists for the production of other C_3H_3O isomers. It has been shown that structure **11** is actually the least stable C_3H_3O isomer and is ∼28 kcal/mol less stable than the 1-oxo-2-propenyl (CH_2═CH−C═O•) radical, as determined by B3LYP/6-311G** level bottom-of-the-well energies by Cooksy.[30]

D. 2-Cyclobuten-1-yl Radical (16) + 2CO Formation. The 2-cyclobuten-1-yl radical (**16**) intermediate is another possible product resulting from the decomposition of the 2-oxepinoxy radical (**1**). Following ring cleavage and CO extrusion (**1** → **7** → **8**) to yield compound **8**, a 1,5-H-migration can occur readily to generate the 5-oxo-2,4-pentadienyl radical (**12**). This relatively stable C_5H_5O isomer can than proceed to **16** along two separate pathways. The first and energetically most feasible pathway is through a rotation to make the 1-oxo-2,4-pentadienyl radical (**14**), followed by ring closure to yield 2-cyclobuten-1-carbonyl radical (**15**), and finally loss of CO to form **16**. The second pathway involves the initial loss of CO from **12** to form the *s-cis*-1,3-butadienyl radical (**13**) and then ring closure to form **16**.

The overall decomposition of the 2-oxepinoxy radical (**1**) to 2-cyclobuten-1-yl radical (**16**) and two CO molecules is endoergic by +20.2 kcal/mol, with the largest absolute activation barrier occurring in the loss of CO from **7** → **8**.

E. Vinyl Radical (18) + Acetylene + 2CO Formation. Vinyl radical (**18**) results from the loss of acetylene from *s-trans*-1,3-butadienyl radical (**17**), which is a rotamer of **13**. At 298 K, the transformation of **17** → **18** is endoergic by +28 kcal/mol and requires ∼41 kcal/mol to overcome the free energy of activation barrier for breakage of the C−C bond. Although a tremendous amount of energy is required at low temperatures, this reaction is expected to become more and more facile as the temperature increases because of the favorable entropy.

F. 2-Cyclopenten-1-yl Radical (19) + CO Formation. Another possible rearrangement of 5-oxo-2,4-pentadienyl radical (**12**) is the 5-endo cyclization to yield the 1-oxo-2-cyclopenten-

TABLE 1: Relative Gibbs Free Energy for All Intermediates and Transition States (298−1250 K) at the B3LYP/6-311+G// B3LYP/6-31G* Level**

structure[a]	E[b] (hartrees/part)	ΔG (298 K) (kcal/mol)	ΔG (500 K) (kcal/mol)	ΔG (750 K) (kcal/mol)	ΔG (1000 K) (kcal/mol)	ΔG (1250 K) (kcal/mol)	$\langle S^2 \rangle$	other (PG, ES, nimag)[c]
1	−382.14542	0.0	0.0	0.0	0.0	0.0	0.78	C_1, 0
TS 1−2	−382.08120	39.4	40.0	41.0	42.0	43.1	0.80	C_1, 1
TS 1−5	−382.06345	49.0	48.8	48.5	48.4	48.3	0.75	C_1, 1
TS 1−7	−382.10117	23.4	21.9	20.1	18.4	16.8	0.78	C_1, 1
2	−382.13066	10.0	10.7	11.6	12.6	13.5	0.78	C_1, 0
TS 2−3	−382.11495	18.6	19.3	20.3	21.4	22.6	0.77	C_1, 1
3	−382.11603	17.3	17.1	16.8	16.4	15.9	0.76	C_1, 0
TS 3−4	−382.11593	16.6	16.5	16.6	16.7	16.9	0.76	C_1, 1
4[d]	−382.16688	−28.1	−36.2	−46.3	−56.2	−66.0	0.77	C_{2v}, $^2B_1$, 0
5	−382.09779	28.9	28.5	27.9	27.3	26.7	0.76	C_1, 0
TS 5−6	−382.09552	29.2	28.7	28.3	27.9	27.7	0.77	C_1, 1
6[e]	−382.12348	0.1	−7.3	−16.4	−25.4	−34.2	0.78	C_1, 0
7	−382.11734	14.1	12.4	10.1	7.8	5.4	0.78	C_1, 0
TS 7−8	−382.05283	50.8	47.9	44.1	40.4	36.7	0.77	C_1, 1
TS 7−20	−382.10567	20.9	19.6	18.0	16.5	15.1	0.78	C_1, 1
8[e]	−382.05766	36.6	26.9	14.8	2.7	−9.3	0.77	C_1, 0
TS 8−9[e]	−382.04579	44.2	35.3	24.3	13.6	3.1	0.77	C_1, 1
TS 8−12[e]	−382.05037	40.0	31.7	21.3	11.0	1.0	0.76	C_1, 1
9[e]	−382.05552	39.0	29.9	18.5	7.3	−3.9	0.77	C_1, 0
TS 9−6[e]	−382.05290	41.7	33.9	24.3	15.0	5.9	0.76	C_1, 1
TS 9−10[e]	−382.04940	41.8	32.8	21.7	10.8	0.1	0.77	C_1, 1
10[e]	−382.05664	38.8	29.9	18.6	7.5	−3.4	0.77	C_1, 0
TS 10−11[e]	−381.98365	79.0	68.2	54.6	41.1	27.7	0.77	C_1, 1
11[f]	−381.99022	65.7	49.0	28.2	7.5	−13.0	0.76	C_1, 0
12[e]	−382.11107	4.3	−4.8	−16.4	−27.8	−39.2	0.78	C_1, 0
TS 12−13[e]	−382.04672	39.8	28.6	14.6	0.7	−12.9	0.77	C_1, 1
TS 12−14[e]	−382.09848	12.0	3.4	−7.1	−17.5	−27.6	0.78	C_1, 1
TS 12−19[e]	−382.09360	16.3	8.3	−1.4	−10.9	−20.2	0.76	C_1, 1
13[g]	−382.04994	27.9	10.7	−10.8	−32.1	−53.1	0.77	C_s, $^2A'$, 0
TS 13−16[g]	−382.00501	57.3	41.8	22.6	3.7	−14.7	0.80	C_1, 1
TS 13−17[g]	−382.04425	32.5	16.6	−3.1	−22.4	−41.2	0.76	C_1, 1
14[e]	−382.11242	3.3	−6.0	−17.7	−29.3	−40.8	0.78	C_1, 0
TS 14−15[e]	−382.04169	47.1	38.5	27.9	17.5	7.3	0.78	C_1, 1
15[e]	−382.07217	30.3	21.9	11.4	1.1	−9.1	0.75	C_1, 0
TS 15−16[e]	−382.05373	39.1	29.9	18.7	7.7	−3.1	0.77	C_1, 1
16[g]	−382.06640	20.2	4.6	−14.8	−33.9	−52.8	0.78	C_1, 0
17[g]	−382.05497	26.2	9.8	−10.6	−30.7	−50.6	0.75	C_s, $^2A'$, 0
TS 17−18[g]	−381.98002	67.0	48.4	25.0	1.9	−20.9	0.77	C_s, $^2A'$, 1
18[h]	−381.98778	54.2	30.5	0.9	−28.4	−57.3	0.76	C_s, $^2A'$, 0
19[e]	−382.14118	−11.7	−19.3	−28.7	−37.9	−47.0	0.78	C_1, 0
20	−382.12212	10.9	8.9	6.4	3.7	1.1	0.78	C_1, 0
TS 20−21	−382.06082	47.2	46.2	44.8	43.5	42.2	0.76	C_1, 1
TS 20−23	−382.09945	24.2	22.6	20.5	18.6	16.7	0.76	C_1, 1
TS 20−26	−382.03754	61.2	59.7	57.7	55.7	53.8	0.76	C_1, 1
TS 20−28	−382.10755	19.5	18.1	16.3	14.6	13.1	0.78	C_1, 1
21	−382.09847	25.0	22.5	19.3	16.1	12.8	0.77	C_1, 0
TS 21−22	−382.04013	55.5	50.6	44.4	38.2	32.1	0.77	C_1, 1
22[i]	−382.04024	46.7	36.6	23.9	11.5	−0.8	0.00	C_1, 0
23	−382.12716	7.7	5.9	3.4	0.9	−1.6	0.78	C_1, 0
TS 23−24	−382.06786	42.4	41.1	39.4	37.8	36.1	0.76	C_1, 1
24	−382.09969	24.6	22.3	19.3	16.2	13.1	0.75	C_1, 0
TS 24−25	−382.04922	51.2	47.1	41.7	36.3	31.0	0.76	C_1, 1
25[j]	−382.04685	42.3	32.0	19.0	6.1	−6.6	0.00	C_1, 0
26	−382.10196	22.4	19.7	16.1	12.4	8.7	0.75	C_1, 0
TS 26−27	−382.02918	63.0	58.8	53.3	47.8	42.2	0.77	C_1, 1
27[k]	−382.03779	47.5	37.2	24.2	11.4	−1.3	0.76	C_1, 0
28	−382.12971	7.3	6.1	4.4	2.7	1.0	0.77	C_1, 0
TS 28−5	−382.07450	42.0	41.7	41.3	41.0	40.8	0.76	C_1, 1
TS 28−10	−382.05540	48.6	45.1	40.7	36.3	32.0	0.77	C_1, 1
TS 28−29	−382.09440	26.8	24.9	22.6	20.3	18.1	0.76	C_1, 1
29	−382.13065	6.1	4.6	2.5	0.3	−1.8	0.77	C_1, 0
TS 29−30	−382.08726	33.7	33.1	32.5	32.0	31.5	0.76	C_1, 1
30	−382.10528	22.9	22.1	20.9	19.6	18.3	0.77	C_1, 0
TS 30−31	−382.06602	45.7	44.3	42.5	40.8	39.1	0.76	C_1, 1
31[j]	−382.06619	34.2	25.8	15.5	5.5	−4.4	0.00	C_s, $^1A'$, 0

[a] See Figure 2 for structures. [b] Bottom-of-the-well energy. [c] Point group (PG), electronic state (ES), and number of imaginary vibrational frequencies (nimag). [d] E and $\Delta G(T)$ values include E and $G(T)$ of CO_2. [e] E and $\Delta G(T)$ values include E and $G(T)$ of CO. [f] E and $\Delta G(T)$ values include E and $G(T)$ of CO and C_2H_2. [g] E and $\Delta G(T)$ values include E and $G(T)$ of 2CO. [h] E and $\Delta G(T)$ values include E and $G(T)$ of 2CO and C_2H_2. [i] E and $\Delta G(T)$ values include E and $G(T)$ of CHO. [j] E and $\Delta G(T)$ values include E and $G(T)$ of C_2HO. [k] E and $\Delta G(T)$ values include E and $G(T)$ of C_2H_2O.

1-yl radical (**19**). The ΔG(298 K) of this reaction is −16.0 kcal/mol, with a $\Delta G^{\ddagger}$(298 K) of 12.0 kcal/mol calculated at the B3LYP/6-311+G**//B3LYP/6-31G* level, both of which compare reasonably well to reported bottom-of-the-well energies

TABLE 2: Relative Energies (kcal/mol) at Different Theoretical Levels for a Few Important Intermediates and Transition States[a,b]

	1	TS 1−2	2	TS 1−7	7	TS 7−8	TS 7−20	20	TS 20−23	TS 20−28	28	TS 28−10
UMP2/6-31G**	0.0	35.4	−11.2	22.9	22.3	61.9	24.0	19.5	17.6	18.6	14.2	60.4
UMP3/6-31G**	0.0	37.7	−6.0	27.9	24.4	61.4	25.9	21.4	24.0	23.6	17.6	59.5
UMP4(SDQ)/6-31G**	0.0	37.1	−5.3	25.3	21.9	56.8	24.0	19.0	22.5	21.2	15.2	55.1
UCCSD/6-31G**	0.0	36.6	−0.1	29.9	22.5	52.5	25.7	19.9	29.9	25.9	16.9	51.6
UCCSD(T)/6-31G**	0.0	35.1	0.0	29.8	22.2	52.2	26.1	19.8	29.7	26.0	16.1	51.7
UB3LYP/6-311+G**	0.0	40.3	9.3	27.8	17.6	58.1	24.9	14.6	28.8	23.8	9.9	56.5
UB3LYP/6-31G*	0.0	41.0	9.2	32.8	22.2	63.4	29.6	19.4	34.0	29.0	13.6	61.5
UB3LYP/6-311+G** $\langle S^2 \rangle$	0.78	0.80	0.78	0.78	0.78	0.77	0.78	0.78	0.76	0.78	0.77	0.77
UCCSD(T)/6-31G** $\langle S^2 \rangle$	1.27	1.36	0.97	1.06	1.23	1.53	1.15	1.22	0.87	1.05	1.17	1.56

[a] The B3LYP/6-31G* geometry was used in each case. The relative energies are at the bottom of the well. [b] See Figure 2 for structures.

calculated at the UHF/6-31G* level of −18.9 and 10.9 kcal/mol, respectively.[31]

G. 1,2,4-Pentatrien-1-one (22) + Formyl Radical Formation. Rotation about the C_2-C_3 bond in (2*Z*,4*Z*)-1,6-dioxo-2,4-hexadienyl radical (**7**) results in a more stable (2*E*,4*Z*)-1,6-dioxo-2,4-hexadienyl radical isomer (**20**). Following a 1,4-H-migration, 1,6-dioxo-1,3-hexadien-2-yl radical (**21**) can be produced. Formyl (HCO) radical extrusion from **21** ends the exploration of this pathway with the formation of 1,2,3-pentatrien-1-one (**22**). This mechanism is endoergic by +35.8 kcal/mol and possesses significant activation barriers for the 1,4-H-migration and the C−C bond breakage to extrude formyl radical.

H. Vinyl ketone (25) + Ketenyl Radical Formation. The most advantageous pathway for the decomposition of **20** yields vinyl ketone (**25**) and ketenyl radical (•HC═C═O). This transformation occurs by the rearrangement of **20** to its rotamer, **23**, followed by a 1,4-H-migration to give **24**, and finally a C−C bond scission that extrudes the ketenyl radical. This pathway is ∼4 kcal/mol less endoergic than the aforementioned pathway for 1,2,4-pentatrien-1-one (**22**) formation. The barrier for the 1,4-H-migration is once again ∼35 kcal/mol, but the barrier for C−C bond breakage is ∼10 kcal/mol lower for ketenyl radical formation than for formyl radical formation.

I. 4-Oxo-1,3-butadienyl Radical (27) + Ketene Formation. The final pathway originating with **20** that was examined involves an unlikely 1,2-H-migration to create the 1,6-dioxo-3,5-hexadienyl radical (**26**), followed by the loss of ketene (CH_2═C═O). This mechanism is the least favorable of the pathways that originate at **20**. For the 1,2-H-migration to occur, ∼50 kcal/mol is required to overcome the free energy of activation barrier.

J. Furan (31) + Ketenyl Radical Formation. The final pathway considered involves the rearrangement and simple decomposition of a rotamer of **7**, the (2*E*,4*Z*)-1,6-dioxo-2,4-hexadienyl radical (**28**). Following two subsequent C−C rotations for **7** → **20** → **28**, structure **28** can rotate around carbon-3 to form an even more stable isomer of **7**, which is compound **29**. A 5-endo cyclization of **29** yields 1-hydrofuran-2-yl ketene radical (**30**). The loss of the ketenyl radical (•HC═C═O) then provides a route for the formation of furan **(31)**.

IV. Comparison of Theoretical Levels

To evaluate the quantitative accuracy of the B3LYP energies, we have also calculated single-point energies at the UCCSD(T)/6-31G** level for some key intermediates and transition states. These relative energies (at the bottom of the well) are provided in Table 2. The UCCSD(T) energies are in qualitative and reasonable quantitative agreement with the B3LYP results. The average difference between the B3LYP/6-311+G**//B3LYP/6-31G* and the UCCSD(T)/6-31G**//B3LYP/6-31G* relative energies is ∼4.0 kcal/mol for all of the structures calculated in Table 2. A major contribution to the magnitude of this variance is the excessive spin contamination in the UCCSD(T)/6-31G**

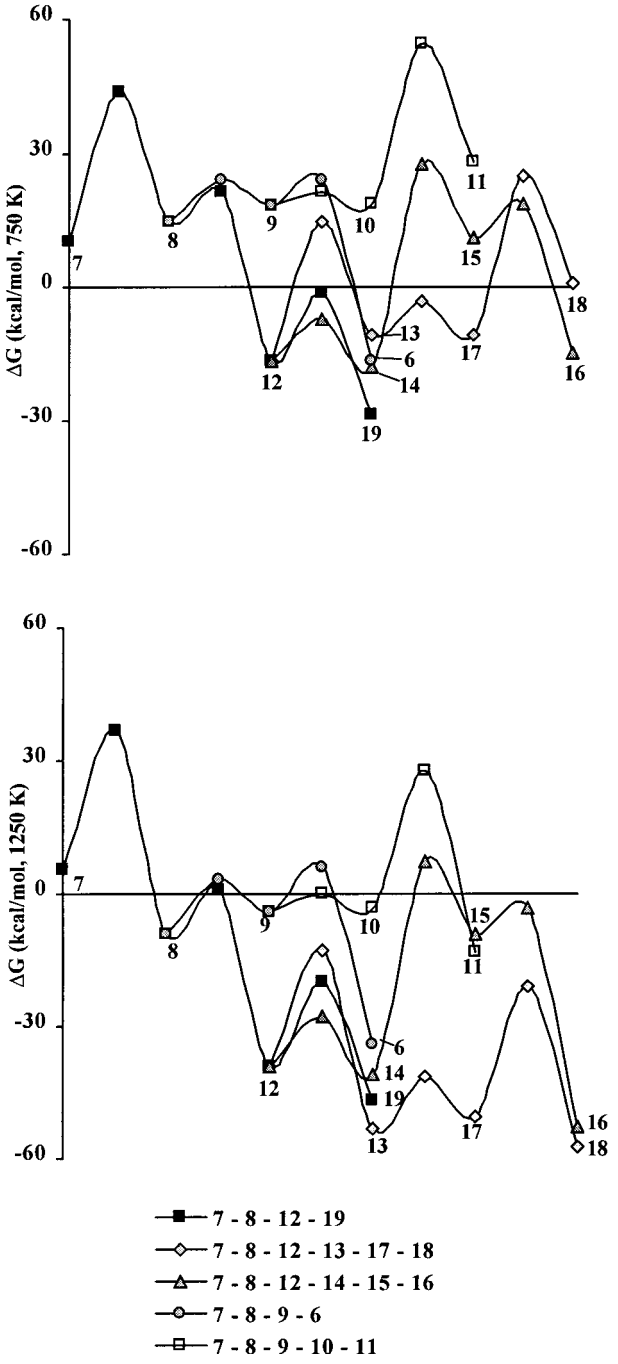

Figure 3. Unimolecular decomposition pathways (top, 750 K; bottom, 1250 K) of 2-oxepinoxy radical (**1**) from intermediate **7** at the B3LYP/6-311+G**//B3LYP/6-31G* level. See Figure 2 for structures.

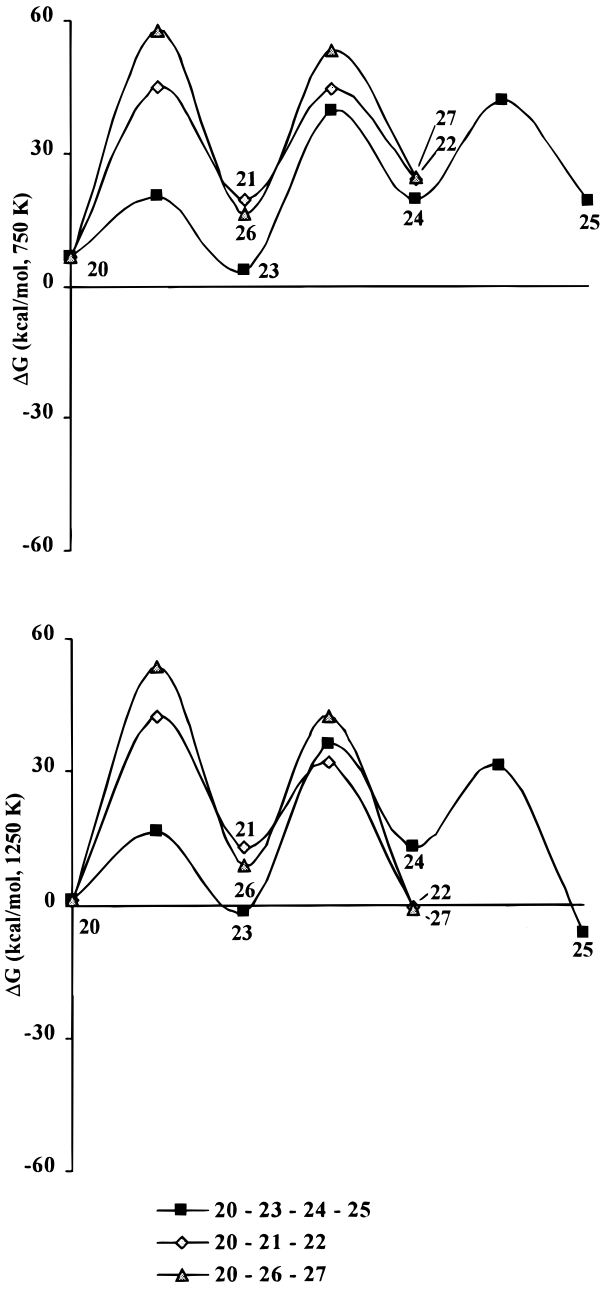

Figure 4. Unimolecular decomposition pathways (top, 750 K; bottom, 1250 K) of 2-oxepinoxy radical (**1**) from intermediate **20** at the B3LYP/6-311+G**//B3LYP/6-31G* level. See Figure 2 for structures.

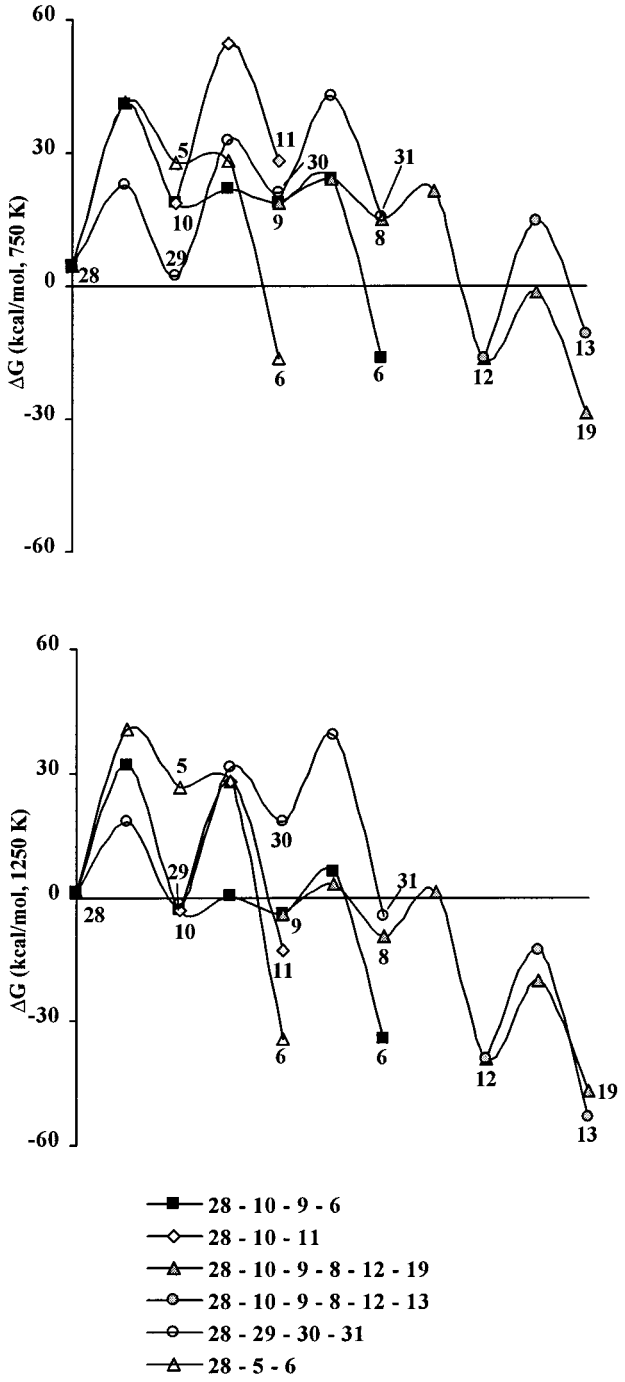

Figure 5. Unimolecular decomposition pathways (top, 750 K; bottom, 1250 K) of 2-oxepinoxy radical (**1**) from intermediate **28** at the B3LYP/6-311+G**//B3LYP/6-31G* level. See Figure 2 for structures.

calculation of the 2-oxepinoxy radical (**1**), the molecule from which all of the relative energies are then compared. In our previous studies,[13,32,33] the UCCSD(T) and B3LYP energies are usually in reasonable agreement when spin contamination is not a problem for the Hartree−Fock-based method.

V. Comparison of Reaction Pathways as a Function of Temperature

To compare reaction pathways as a function of temperature, we have plotted the relative Gibbs free energy profiles of the intermediates and transition states in Figures 3−6 for the possible mechanisms discussed above and shown schematically in Figure 2. All references to energies or activation barriers in this section refer to Gibbs free energies and free energy of activation barriers, and these energies are also provided in Table 1. First, energy profiles will be examined for the decomposition pathways leading from **7** (Figure 3), **20** (Figure 4), and **28** (Figure 5). Then, the most accessible pathways from each of these will be compared to the decomposition pathways of **1** leading to **4** and **6** (Figure 6).

Rearrangement and simple unimolecular decomposition of **7** can yield the products of **6** + CO, **11** + C_2H_2 + CO, **16** + 2 CO, **18** + C_2H_2 + 2 CO, and **19** + CO, as shown in Figures 2 and 3. At temperatures ≤1000 K, the most stable products are the 1-oxo-2-cyclopenten-1-yl radical (**19**) and CO. By 1250 K, formation of the vinyl radical (**18**), acetylene, and two CO molecules is ∼10 kcal/mol more stable than **19** + CO. The key activation barriers to contrast are **TS 8−9** with **TS 8−12** and **TS 12−13** with **TS 12−19**. **TS 8−12** is lower in energy at all

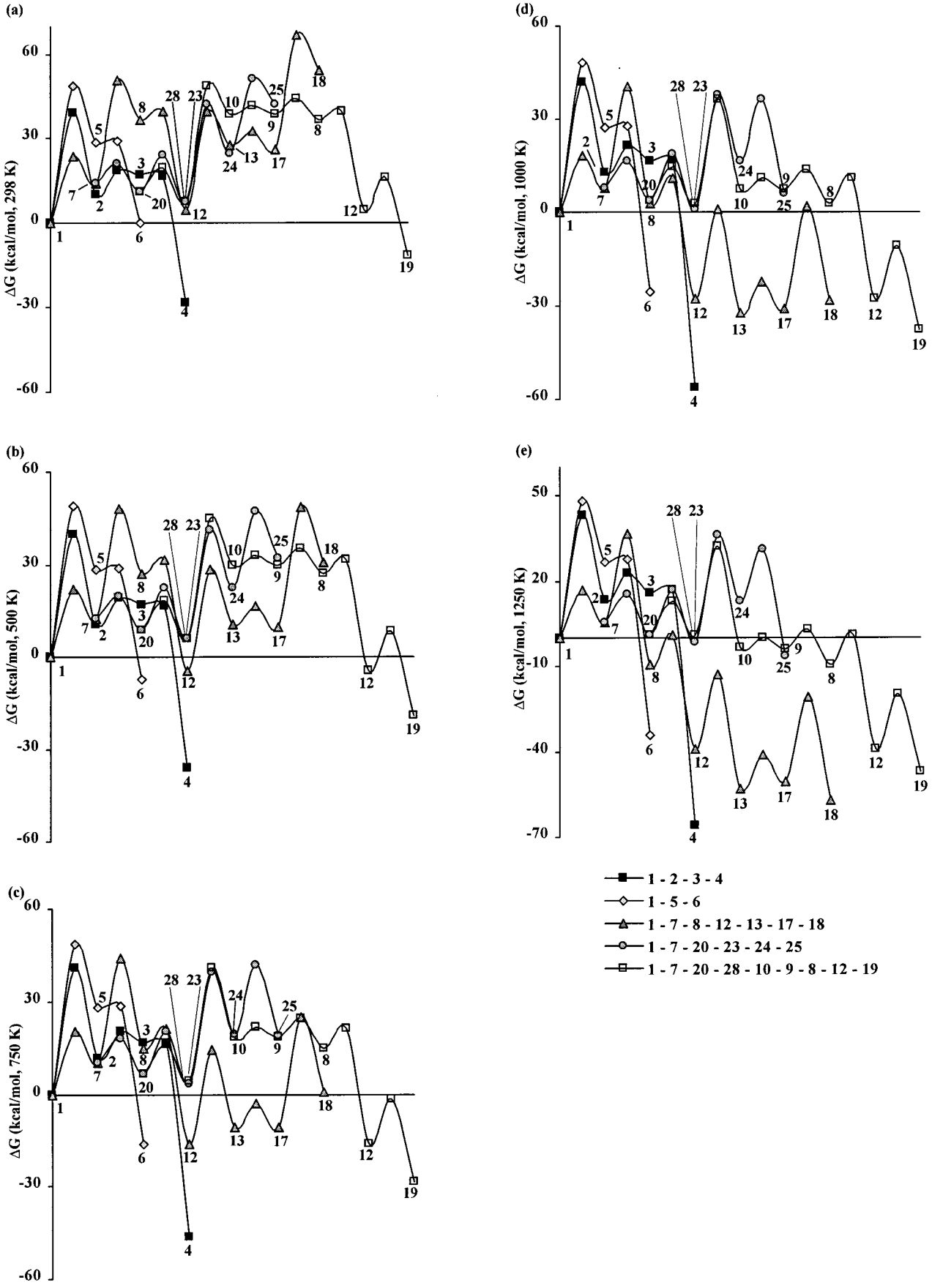

Figure 6. Comparison of the relative Gibbs free energy profiles of the most accessible pathways from Figures 3−5 against direct pathways leading to cyclopentadienyl radical (**4**) and pyranyl radical (**6**) at (a) 298, (b) 500, (c) 750, (d) 1000, and (e) 1250 K at the B3LYP/6-311+G**//B3LYP/6-31G* level. See Figure 2 for structures.

TABLE 3: Relative Gibbs Free Energy for All Intermediates for the Oxidation of Cyclopentadienyl Radical (298−1250 K) at the B3LYP/6-311+G//B3LYP/6-31G* Level**

structure[a]	E^b (hartrees/part)	ΔG (298 K) (kcal/mol)	ΔG (500 K) (kcal/mol)	ΔG (750 K) (kcal/mol)	ΔG (1000 K) (kcal/mol)	ΔG (1250 K) (kcal/mol)	$\langle S^2 \rangle$	other (PG, ES, nimag)[c]
A[d]	−193.51822	0.0	0.0	0.0	0.0	0.0	0.77	C_{2v}, $^2B_1$, 0
B	−343.90509	5.7	14.0	24.2	34.2	44.4	0.75	C_1, 0
C	−343.92461	−7.5	0.3	9.7	18.9	28.0	0.76	C_1, 0
D	−343.29405	61.7	65.2	69.1	72.8	76.3	0.00	C_1, 0
E[e]	−268.35459	−34.1	−33.6	−32.5	−31.4	−30.3	0.00	C_1, 0
E[f]	−268.18434	62.5	58.4	53.4	48.2	42.8	0.00	C_1, 0
F[g]	−343.31056	51.5	55.1	59.3	63.1	66.8	0.00	C_1, 0
G[g]	−343.26548	80.3	84.3	88.9	93.2	97.4	0.00	C_1, 0
H[g]	−343.15258	149.7	152.7	156.6	160.1	163.5	0.00	C_1, 0

[a] See Figure 7 for structures. [b] Bottom-of-the-well energy. [c] Point group (PG), electronic state (ES), and number of imaginary vibrational frequencies (nimag). [d] $\Delta G(T)$ values include $G(T)$ of O_2. [e] $\Delta G(T)$ values include $G(T)$ of OH radical. [f] $\Delta G(T)$ values include $G(T)$ of H and $O(^3P)$. [g] $\Delta G(T)$ values include $G(T)$ of $O(^3P)$.

temperatures studied than **TS 8−9**; however, the difference in free energy between the two structures erodes from ∼4 kcal/mol at 298 K to ∼2 kcal/mol at 1250 K. As the temperature increases, the barrier to the formation of **13** from **12** decreases sharply as compared to the barrier between **12** and **19**. In conclusion, at temperatures ≤1000 K, the dominant product from the decomposition of **7** should be **19**, but at higher temperatures, the decomposition of **17** to yield vinyl radical (**18**), acetylene, and two CO molecules will begin to dominate.

The rearrangement and further decomposition of **20** can yield **22** + formyl radical, **25** + ketenyl radical, or **27** + ketene, as shown in Figures 2 and 4. The most stable product, vinylketene (**25**) and ketenyl radical, also exhibits the lowest overall barrier at all temperatures examined. Even though this mechanism is only slightly exoergic with respect to the 2-oxepinoxy radical (**1**) and only at high temperatures (>1000 K), the production of vinylketene (**25**) from the decomposition of **20** will be the most favored product of the pathways studied.

As shown in Figure 2, the decomposition pathways of **28** merge into the pathways for the decomposition of **7**. The only differences are the pathways for the production of furan (**31**) and ketenyl radical and for pyranyl radical (**6**) and CO formation. At temperatures ≤500 K (Table 1), the pathway leading to pyranyl radical (**6**) formation exhibits the lowest overall activation barrier. At higher temperatures, the pathways discussed in the decomposition of **7** will dominate (Figures 3 and 5).

A comparison of the lowest Gibbs free energy pathways for the decomposition of **7**, **20**, and **28** with the direct decomposition of the 2-oxepinoxy radical (**1**) to cyclopentadienyl radical (**4**) and pyranyl radical (**6**) reveals several important trends (Figure 6). First, at temperatures below 1000 K, the most favored pathway is **1** → **2** → **3** → **4**, resulting in the generation of cyclopentadienyl radical and CO_2. At temperatures ranging from 1000 to 1250 K, the major product channels result in formation of the 5-oxo-2-cyclopenten-1-yl radical (**19**), with CO and also vinyl radical (**18**), acetylene, and two CO molecules. The 5-oxo-2-cyclopenten-1-yl radical (**19**) is a possible precursor to cyclopentadienone (C_5H_4O), and therefore, cyclopentadienone can be formed via the unimolecular decomposition of phenylperoxy ($C_6H_5OO^•$) radical directly and not only through the further oxidation of cyclopentadienyl radical (**4**) as an intermediate. Judging from the Gibbs free energy profiles, the mechanism leading to vinyl radical (**18**), acetylene, and two CO molecules at 1250 K is a major pathway for the decomposition of the 2-oxepinoxy radical (**1**) and, therefore, possibly a major pathway for the unimolecular decomposition of phenylperoxy ($C_6H_5OO^•$) radical. This pathway provides a mechanism that proceeds through $C_6 \rightarrow C_5 \rightarrow C_4 \rightarrow C_2$ intermediates, but does not include the cyclopentadienyl radical as a precursor.

VI. Comparison of Pathways for Cyclopentadienone Formation

Cyclopentadienone (C_5H_4O) is a possible intermediate formed during the oxidation of benzene under combustion conditions. Its mass/charge ratio has been observed in several experimental mass spectrometric studies of benzene combustion.[7,9] The prevalent explanation for cyclopentadienone formation is that it is generated by the oxidation of cyclopentadienyl radical (**4**). Wang and Brezinsky, using the semiempirical PM3 method and the Gaussian-2 method for related compounds, examined the feasiblity of cyclopentadienone production from the oxidation of cyclopentadienyl radical with O atom or O_2.[34] They concluded that both reactions are exoergic. In a related study, Bozzelli modeled the reactions of cyclopentadienyl radical with H, OH, O, and O_2.[35] They concluded that oxidation of $Cp^•$ with O can lead to cyclopentadienone, but the addition of O_2 to $Cp^•$ generally results in reversion back to the reactants.[35]

We examined the oxidation of cyclopentadienyl radical (**A**) with O_2 using the B3LYP method by calculating the Gibbs free energy of the reactant (**A**), several intermediates (**B**−**D**, **F**−**H**), and cyclopentadienone (**E**), as shown in Table 3 and Figure 7. Our calculations show that the initial reaction for O_2 addition to cyclopentadienyl radical is endoergic at all temperatures (≤1250 K), with the reaction becoming less favorable as the temperature increases. Also, the intermediate **C**, resulting from a 1,3-H-migration in **B**, is the most stable intermediate. The **B** → **C** rearrangement is exoergic throughout the temperature range of 298 to 1250 K, and this step is followed by another exoergic reaction, the loss of hydroxyl radical ($HO^•$) to yield cyclopentadienone (**E**). Although the first reaction is endoergic, the overall reaction of cyclopentadienyl radical (**A**) with O_2 to yield cyclopentadienone and $HO^•$ is exoergic by ≥30 kcal/mol at temperatures ≤1250 K.

H-atom loss from **B** to generate **D** (Figure 7) is very endoergic. Structure **D** does provide a route to 1,1- (dioxiranyl, **F**), 1,2- (dioxetanyl, **G**), or 1,3-addition (**H**) intermediates; however, the large endoergicity of the **B** → **D** transformation makes these routes to not be viable.

Based on the presumption that cyclopentadienone is a prevalent intermediate in the thermal oxidation of benzene and the computational evidence for the highly endoergic nature of the initial step for oxidation of cyclopentadienyl radical at high temperatures, the possibility of an alternative mechanism for cyclopentadienone formation seems likely. In Figure 8, we compare three pathways for the production of cyclopentadienone at 1250 K.

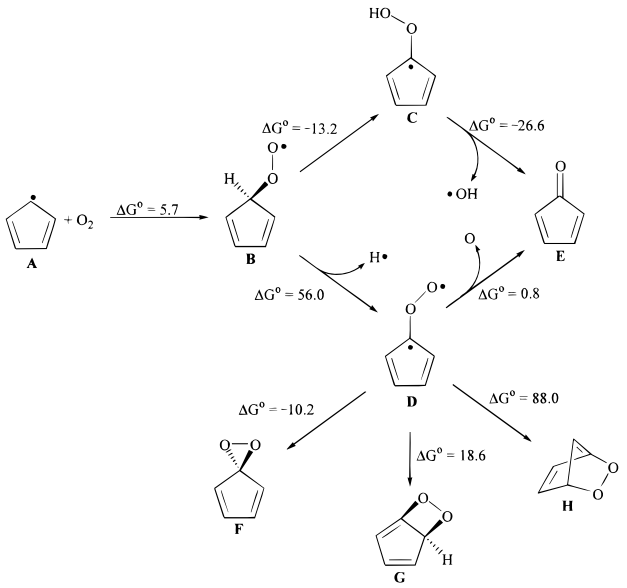

Figure 7. Oxidation and subsequent decomposition of cyclopentadienyl radical (**A**). The relative free energies (298 K, kcal/mol) at the B3LYP/6-311+G**//B3LYP/6-31G* level are shown for each intermediate relative to **A**.

The first pathway involves the decomposition of phenylperoxy ($C_6H_5OO^\bullet$) radical to the phenoxy ($C_6H_5O^\bullet$) radical, the subsequent rearrangement and decomposition to cyclopentadienyl radical and CO,[13] followed by the oxidation of cyclopentadienyl radical (as discussed above), ultimately leading to cyclopentadienone (C_5H_4O, **E**) and hydroxyl radical formation. Although this sequence, with an overall stoichiometry of

$$C_6H_5O_2^\bullet + O_2 \rightarrow\rightarrow C_5H_4O + CO + HO^\bullet + O(^3P)$$

is exoergic by −63.1 kcal/mol, the mechanism contains two individual steps that are endoergic by >40 kcal/mol at 1250 K. These steps are the rearragement of phenoxy radical to a bicyclic species[13] and the oxidation of cyclopentadienyl radical.

The second possible pathway proceeds via isomerization of phenylperoxy ($C_6H_5OO^\bullet$) radical to 2-oxepinoxy radical (**1**), followed by ring scission, CO extrusion, hydrogen migration, and ring closure to form 5-oxo-2-cyclopenten-1-yl radical (**19**), as described above. The final step would be H-atom abstraction from **19** to form cyclopentadienone (**E**). This reaction

$$C_6H_5O_2^\bullet \rightarrow\rightarrow C_5H_4O + CO + H^\bullet$$

is exoergic by −71.3 kcal/mol at 1250 K, with the final H-atom abstraction step being the least energetically favored (+25.4 kcal/mol). Of course, this last step could be facilitated energetically by a good H-atom abstracting agent, such as $HO^\bullet$ radical, which would generate water as a product.

The final pathway is an amalgamation of the first two pathways. This mechanism includes the isomerization step of pathway 2,[13] followed by CO_2 extrusion to generate **4** (i.e., $C_6H_5O_2^\bullet \rightarrow$ **1** $\rightarrow$ **2** $\rightarrow$ **3** $\rightarrow$ **4**) and then oxidation of cyclopentadienyl radical (**4**) and further decomposition, as detailed in pathway 1. This combined pathway for the overall reaction

$$C_6H_5O_2^\bullet + O_2 \rightarrow\rightarrow C_5H_4O + CO_2 + HO^\bullet$$

benefits from the greatest overall change in Gibbs free energy at 1250 K of −145.9 kcal/mol. It suffers, though, from the high activation barriers in the individual steps for the formation of the bicyclic structure (**2**) from the rearrangement of 2-oxepinoxy radical (**1**) and from the endoergic reaction of cyclopentadienyl radical (**4**) with O_2 to generate the $C_5H_5O_2$ radical (**B**).

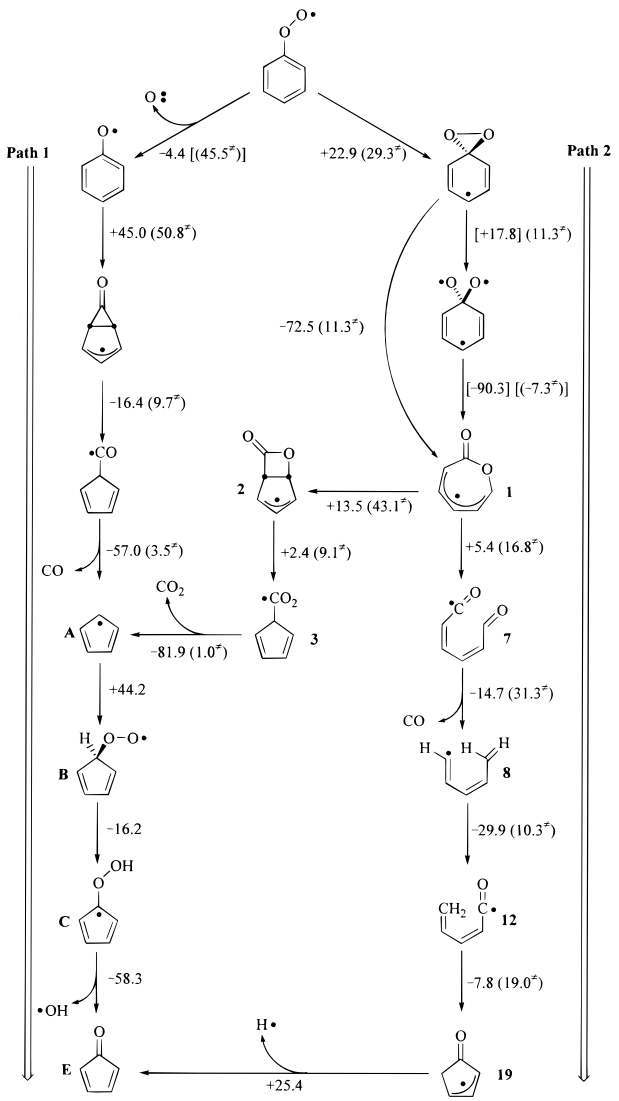

Figure 8. Comparison of reaction pathways for the production of cyclopentadienone from phenylperoxy radical at 1250 K. The free energy and free energy of activation (in parentheses) for each step (1250 K, kcal/mol) at the B3LYP/6-311+G**//B3LYP/6-31G* level is shown. Values in brackets are suspect because of excess spin contamination in the calculations. Values for phenylperoxy radical decomposition along path 1 to cyclopentadienyl radical and along path 2 to 2-oxepinoxy radical are taken from ref 13.

VII. Conclusions

The Gibbs free energy profiles of the unimolecular decomposition of the 2-oxepinoxy radical at temperatures ranging from 298 to 1250 K have been obtained using the B3LYP method. Intermediates and transition states have been obtained that link the 2-oxepinoxy radical (**1**) to various products that have been experimentally observed during the thermal oxidation of benzene.

The decomposition of 2-oxepinoxy radical (**1**) along the pathways examined provides a mechanism that proceeds from $C_6 \rightarrow C_5 \rightarrow C_4 \rightarrow C_2$ intermediates, but does not include the cyclopentadienyl radical as an intermediate. These pathways provide an alternate route for the formation of the key intermediates C_4H_5, C_5H_4O, and C_3H_3O aside from the oxidation

of cyclopentadienyl radical. The most viable pathway (**1** → **7** → **8** → **12** → → **18** or **19**) at temperatures between 1000 and 1250 K produces either 5-oxo-2-cyclopenten-1-yl radical (**19**) and CO or vinyl radical (**18**), acetylene, and two molecules of CO. The mechanism to form **19**, a possible precursor to cyclopentadienone, is competitive with cyclopentadienone formation from the decomposition of phenoxy radical to cyclopentadienyl radical, followed by oxidation and rearrangement.

Acknowledgment. We gratefully acknowledge the U.S. Department of Energy (Grant DE-FG22-96PC96249), the Ohio Supercomputer Center, and the U.S. Army for support of this research. We also thank Paul R. Rablen (Swarthmore College) for providing his Thermo94 program.

Supporting Information Available: Energies, enthalpies, free energies as a function of temperature, and moments of inertia for all intermediates and transition states. Cartesian coordinates and harmonic vibrational frequencies for all intermediates and transition states for each aryl radical with O_2. This material is available free of charge via the Internet at http://pubs.acs.org.

References and Notes

(1) Fujii, N.; Asaba, T. *Symp. (Int.) Combust., 14th* **1973**, 433−442.
(2) Fujii, N.; Asaba, T.; Miyama, H. *Acta Astron.* **1974**, *1*, 417−426.
(3) Hsu, D. S. Y.; Lin, C. Y.; Lin, M. C. *Symp. (Int.) Combust., 20th* **1984**, 623−630.
(4) Venkat, C.; Brezinsky, K.; Glassman, I. *Symp. (Int.) Combust., 19th* **1982**, 143−152.
(5) Bittker, D. A. *Combust. Sci. Technol.* **1991**, *79*, 49−72.
(6) Zhang, H. Y.; McKinnon, J. T. *Combust. Sci. Technol.* **1995**, *107*, 261−300.
(7) Rotzoll, G. *Int. J. Chem. Kinet.* **1985**, *17*, 637−653.
(8) Bermudez, G.; Pfefferle, L. *Combust. Flame* **1995**, *100*, 41−51.
(9) Chai, Y.; Pfefferle, L. D. *Fuel* **1998**, *77*, 313−320.
(10) Sethuraman, S.; Senkan, S. M.; Gutman, D. *Combust. Sci. Technol.* **1992**, *82*, 13−30.
(11) Carpenter, B. K. *J. Am. Chem. Soc.* **1993**, *113*, 9806−9807.
(12) Barckholtz, C.; Fadden, M. J.; Hadad, C. M. *J. Phys. Chem. A* **1999**, *103*, 8108−8117.
(13) Fadden, M. J.; Hadad, C. M. *J. Phys. Chem. A* **2000**, *104*, 3004−3011.
(14) Mebel, A. M.; Lin, M. C.; Yu, T.; Morokuma, K. *J. Phys. Chem. A* **1997**, *101*, 3189−3196.
(15) Barckholtz, C.; Barckholtz, T. A.; Hadad, C. M. *J. Am. Chem. Soc.* **1999**, *121*, 491−500.
(16) Frisch, M. J.; Trucks, G. W.; Schlegel, H. B.; Gill, P. M. W.; Johnson, B. G.; Robb, M. A.; Cheeseman, J. R.; Keith, T.; Petersson, G. A.; Montgomery, J. A.; Raghavachari, K.; Al-Laham, M. A.; Zakrzewski, V. G.; Ortiz, J. V.; Foresman, J. B.; Cioslowski, J.; Stefanov, B. B.; Nanayakkara, A.; Challacombe, M.; Peng, C. Y.; Ayala, P. Y.; Chen, W.; Wong, M. W.; Andres, J. L.; Replogle, E. S.; Gomperts, R.; Martin, R. L.; Fox, D. J.; Binkley, J. S.; Defrees, D. J.; Baker, J.; Stewart, J. J. P.; Head-Gordon, M.; Gonzalez, C.; Pople, J. A. *Gaussian 94*, revision D.3; Gaussian, Inc.; Pittsburgh, PA, 1995.
(17) Frisch, M. J.; Trucks, G. W.; Schlegel, H. B.; Scuseria, G. E.; Robb, M. A.; Cheeseman, J. R.; Zakrzewski, V. G.; Montgomery, J. A., Jr.; Stratmann, R. E.; Burant, J. C.; Dapprich, S.; Millam, J. M.; Daniels, A. D.; Kudin, K. N.; Strain, M. C.; Farkas, O.; Tomasi, J.; Barone, V.; Cossi, M.; Cammi, R.; Mennucci, B.; Pomelli, C.; Adamo, C.; Clifford, S.; Ochterski, J.; Petersson, G. A.; Ayala, P. Y.; Cui, Q.; Morokuma, K.; Malick, D. K.; Rabuck, A. D.; Raghavachari, K.; Foresman, J. B.; Cioslowski, J.; Ortiz, J. V.; Stefanov, B. B.; Liu, G.; Liashenko, A.; Piskorz, P.; Komaromi, I.; Gomperts, R.; Martin, R. L.; Fox, D. J.; Keith, T.; Al-Laham, M. A.; Peng, C. Y.; Nanayakkara, A.; Gonzalez, C.; Challacombe, M.; Gill, P. M. W.; Johnson, B. G.; Chen, W.; Wong, M. W.; Andres, J. L.; Gonzalez, C. Head-Gordon, M.; Replogle, E. S.; Pople, J. A. *Gaussian 98*, revision A.7; Gaussian, Inc.; Pittsburgh, PA, 1998.
(18) (a) Labanowski, J. W.; Andzelm, J. *Density Functional Methods in Chemistry*; Springer: New York, 1991. (b) Parr, R. G.; Yang, W. *Density Functional Theory in Atoms and Molecules*; Oxford University Press: New York, 1989.
(19) Becke, A. D. *Phys. Rev. A* **1988**, *38*, 3098−3100.
(20) Lee, C.; Yang, W.; Parr, R. G. *Phys. Rev. B* **1988**, *37*, 785−789.
(21) Becke, A. D. *J. Chem. Phys.* **1993**, *98*, 1372.
(22) Hehre, W. J.; Radom, L.; Schleyer, P. v. R.; Pople, J. A. *Ab Initio Molecular Orbital Theory*; John Wiley & Sons: New York, 1986.
(23) (a) Cioslowski, J.; Liu, G.; Martinov, M.; Piskorz, P.; Moncrieff, D. *J. Am. Chem. Soc.* **1996**, *118*, 5261−5264. (b) Cioslowski, J.; Liu, G.; Moncrieff, D. *J. Org. Chem.* **1996**, *61*, 4111−4114.
(24) Bauschlicher, C. W., Jr.; Langhoff, S. R. *Mol. Phys.* **1999**, *96*, 471.
(25) Stanton, J. F.; Gauss, J.; Watts, J. D.; Lauderdale, W. J.; Bartlett, R. J. *Int. J. Quantum Chem.* **1992**, *S26*, 879.
(26) Scott, A. P.; Radom, L. *J. Phys. Chem.* **1996**, *100*, 16502−16513.
(27) (a) Gonzalez, C.; Schlegel, H. B. *J. Chem. Phys.* **1989**, *90*, 2154. (b) Gonzalez, C.; Schlegel, H. B. *J. Phys. Chem.* **1990**, *94*, 5523.
(28) Rablen, P. R. *Thermo94*; Yale University: New Haven, CT, 1994.
(29) Chase, M. W., Jr. *NIST-JANAF Thermochemical Tables*; American Chemical Society and American Institute of Physics for the National Institute of Standards and Technology: Washington, D.C., 1998.
(30) Cooksy, A. L. *J. Phys. Chem. A* **1998**, *102*, 3093−3099.
(31) Yamamoto, Y.; Ohno, M.; Eguchi, S. *J. Org. Chem.* **1996**, *61*, 9264−9271.
(32) Fadden, M. J.; Hadad, C. M. *J. Phys. Chem. A* **2000**, *104*, 6088−6094.
(33) Fadden, M. J.; Hadad, C. M. *J. Phys. Chem. A* **2000**, *104*, 6324−6331.
(34) Wang, H.; Brezinsky, K. *J. Phys. Chem. A* **1998**, *102*, 1530−1541.
(35) Zhong, X.; Bozzelli, J. W. *J. Phys. Chem. A* **1998**, *102*, 3537−3555.